Biochemistry and Biophysics Reports 29 (2022) 101199

Contents lists available at ScienceDirect

Biochemistry and Biophysics Reports

journal homepage: www.elsevier.com/locate/bbrep

Thermal hysteresis in microtubule assembly/disassembly dynamics: The aging-induced degradation of tubulin dimers

R. Wu [a], J.R. Guzman-Sepulveda [a,1], A.P. Kalra [b,2], J.A. Tuszynski [b,c], A. Dogariu [a,*]

[a] CREOL, College of Optics and Photonics, University of Central Florida, Orlando, FL, 32816, USA
[b] Department of Physics, University of Alberta, 11335 Saskatchewan Dr NW, Edmonton, Alberta, T6G 2M9, Canada
[c] DIMEAS, Polytechnic di Torino, Turin, I-10129, Italy

ARTICLE INFO

Keywords:
Microtubule
Tubulin
Hysteresis
Dynamic light scattering

ABSTRACT

The assembly/disassembly of biological macromolecules plays an important role in their biological functionalities. Although the dynamics of tubulin polymers and their super-assembly into microtubule structures is critical for many cellular processes, details of their cyclical polymerization/depolymerization are not fully understood. Here, we use a specially designed light scattering technique to continuously examine the effects of temperature cycling on the process of microtubule assembly/disassembly. We observe a thermal hysteresis loop during tubulin assembly/disassembly, consistently with earlier reports on the coexistence of tubulin and microtubules as a phase transition. In a cyclical process, the structural hysteresis has a kinetic component that depends on the rate of temperature change but also an intrinsic thermodynamic component that depends on the protein topology, possibly related to irreversible processes. Analyzing the evolution of such thermal hysteresis loops over successive cycles, we found that the assembly/disassembly ceases after some time, which is indicative of protein aging leading to its inability to self-assemble after a finite number of temperature cycles. The emergence of assembly-incompetent tubulin could have major consequences for human pathologies related to microtubules, including aging, neurodegenerative diseases and cancer.

1. Introduction

Microtubules (MTs) are hollow cylindrical polymers of α, β tubulin dimers ubiquitously found in eukaryotic cells (Fig. 1a). They are typically several micrometers long and highly rigid (Young's modulus ~ 1 GPa, persistence length 1–10 mm) [1], which allows them to generate force required for chromosomal segregation [2] and cell movement [3]. They also act as interconnected tracks for macromolecular transport over intra-cellular distances [4,5]. The versatility of MT functions is enhanced through their dynamic instability, which permits *en masse* intracellular reorganization *via* large length changes over short periods of time [6].

MTs elongate as randomly diffusing guanosine triphosphate (GTP) bound tubulin dimers bind to both of its ends. Subsequently, the hydrolysis of GTP to guanosine diphosphate (GDP) at β tubulin takes place, leading to the presence of a large number of GDP-bound β tubulins within a single MT. Periods of steady elongation are stochastically interspersed with rapid dissociation events of tubulin dimers from the MT-growing end referred to as 'catastrophes' [7–9]. Early work indicated that the GTP-GDP transition within a MT could lead to the disappearance of a stabilizing GTP-cap, the loss of which could lead to a catastrophe [7,9–12]. However, recent experiments using advanced, single molecule fluorescence microscopy indicate that a catastrophe might involve a more complex, MT age-dependent cascade [13–15]. The relationship between the age of a MT and its plus-end-taper has also been explored [16]. However, the critical influence of MT age on the overall 'polymerizability' of tubulin dimers has not yet been investigated.

In this paper, we use a light scattering technique specifically designed to dynamically quantify the relationship between overall MT mass in a buffer solution containing tubulin dimers, and the number of tubulin polymerization/depolymerization cycles the tubulin pool has

* Corresponding author.
E-mail address: adogariu@creol.ucf.edu (A. Dogariu).
[1] Currently with the Center for Research and Advanced Studies of the National Polytechnic Institute (CINVESTAV Unidad Monterrey). Apodaca, Nuevo Leon, Mexico.
[2] Presently at Department of Chemistry, Princeton University, Princeton, New Jersey 08544, USA.

https://doi.org/10.1016/j.bbrep.2021.101199
Received 1 October 2021; Received in revised form 29 December 2021; Accepted 31 December 2021

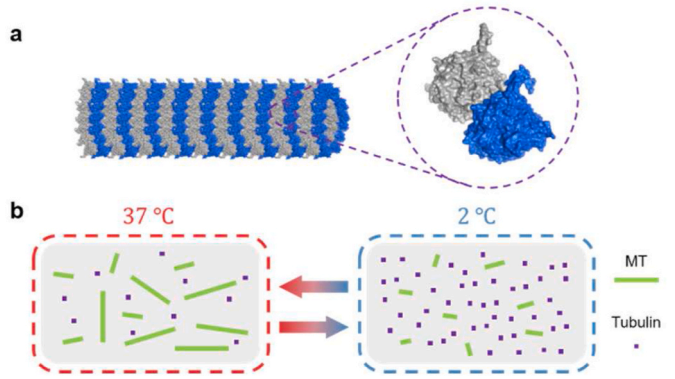

Fig. 1. Illustration of the tubulin-microtubule system. a Cartoon of a microtubule and tubulin dimer (which consists of α, β tubulin monomers). **b** Evolution of an isolated tubulin-microtubule system under temperature modulation. Regardless of the initial condition, the steady state of the system depends on temperature. At high temperature (37 °C), most of tubulin dimers will polymerize into microtubules (green rods), while some tubulin dimers will still diffusive freely (purple dots). At low temperature (2 °C), due to the depolymerization process and dynamic instability of the microtubules, the system will consist of a large number of free tubulin dimers, while a small portion of short microtubules might still be present. (For interpretation of the references to color in this figure legend, the reader is referred to the Web version of this article.)

been subjected to. Compared to traditional turbidity assays, this approach permits not only to retrieve the optical density (turbidity) of a colloidal suspension, but also to discriminate between different populations of scattering centers based on their size and optical cross-section [17]. In an isolated tubulin-MT system, tubulin dimers (at a concentration of 45 μM) are first allowed to polymerize into MTs under appropriate conditions (37 °C, 1 mM GTP). Next, depolymerization is induced by lowering the temperature down to 2 °C (see Fig. 1b) [18]. This is followed by another cycle of polymerization involving temperature increasing to 37 °C. After repeating this process several times, we observe an interesting hysteresis behavior of the total polymerized mass, whose properties can be attributed to the aging of tubulin dimers with further detailed tubulin species analysis.

It is worth mentioning that a phenomenological thermodynamic model of tubulin coexistence with MTs [19] reproduced a phase diagram for this system and predicted the presence of thermal hysteresis, which we experimentally demonstrate in this paper for the first time. This is consistent with a thermodynamic representation of the system of tubulin in solution as manifesting coexistence of two metastable phases of this protein: dispersed (free tubulin) and polymerized (MTs). The relative stability of each phase depends on temperature with low temperature favoring free tubulin while high temperature gradually shifting the balance toward MTs.

2. Materials and methods

Experimental setup. The basic principle and description of the low coherence dynamic light scattering setup is documented in detailed elsewhere [17,20]. Briefly, a super-luminescent diode centered at 670 nm with a coherence length of 30 μm (Superlum, cBLMD-S-670-HP1-SM-1) serves as a light source. The light is coupled into a 2×1 50/50 multimode fiber coupler and illuminated on the sample. The fibers used in these experiments are commercially available 62.5/125 multimode fiber (Fibertronics). The reflected light, which consists of both the Fresnel reflection from the fiber-sample interface and backscattered light from the sample, is captured by the same fiber coupler and directed into the photo-receiver (New Focus 2001-FC). The signal is subsequently digitized by a data acquisition card (Data Translation, DT9832A-02-0-BNC) and processed in the frequency domain using a home-built MATLAB analysis tool. For the cyclical experiment, the integration time of each power spectrum is 30 s and the frequency range is from 1 Hz to 10 kHz, with 1 Hz resolution. The temperature controller is a built-in unit of a commercial dynamic light scattering instrument (Malvern Panalytical, Zetasizer Nano ZS), which is capable of quickly tuning the temperature from 0 to 40 °C with 0.1 °C accuracy. The power at the distal end of the fiber is lower than 2 mW such that the heating effect is negligible.

Sample preparation. The tubulin (porcine brain, >99% pure, T240), GTP (BST06) and BRB80 buffer (BST01) are purchased from Cytoskeleton, Inc (Denvor, CO) and kept at 2 °C until used. The BRB80 buffer, which consists of 80 mM PIPES, 2 mM $MgCl_2$, and 0.5 mM EGTA, is prefiltered with a 0.22 μm size filter before utilized. Microtubule cushion buffer was prepared with the BRB80 buffer and glycerol (60% v/v). The sample was prepared mainly following the standard protocol from Cytoskeleton, Inc. Briefly, first, one aliquot of GTP (2.5 μL, 100 mM) was added to 247.5 μL BRB80 buffer (G-PEM buffer). 180 μL G-PEM buffer is added to one aliquot of tubulin powder (1 mg). Finally, 20 μL of cushion buffer is added to the sample. The final sample, which has a total volume of 200 μL, consists of 45 μM Tubulin as well as 1 mM GTP. The measurement starts immediately after the sample is prepared.

Analysis of the power spectrum. The total energy in the power spectrum of the light intensity fluctuations originates from the dynamical movement of the scattering elements. For monodisperse particles under Brownian motion conditions, it is given by

$$\beta = \int_0^{+\infty} P(f)df = \alpha N \sigma$$

where β denotes the total energy in the light fluctuations, f represents the frequency of the dynamic movement, $P(f)$ is the measured power spectrum, σ is the scattering cross-section of the scattering element, and N is the number density of dynamic elements. α is an experimental constant. For dynamic systems slowly evolving in time, a description of the long-term dynamics can be pursued using a generalized time-frequency i.e. spectrogram, representation of the system's structural dynamics.

For systems consisting of multiple species of scattering elements, the power spectrum of the measured intensity fluctuations can be decomposed into a sum of discrete representative contributions. In this paper, we consider three such contributions and, therefore, the above equation can be generalized as

$$P_n(f) = \frac{P(f)}{\beta} = \sum_{i=1}^{3} P_i(f) = \frac{2}{\pi} \sum_{i=1}^{3} \frac{a_i/\tau_i}{f^2 + (1/\tau_i)^2}$$

with $\sum_{i=1}^{3} a_i(t) = 1$, where a_i and τ_i are the relative amplitude and the characteristic relaxation time, respectively, of each Lorentzian component used in the power spectrum decomposition. $P_n(f)$ is the normalized measured power spectrum, and $P_i(f)$ is the power spectrum of the i-th population. For each species, an effective diffusion coefficient can be inferred as.

$$D_{eff,i} = \frac{k_B T}{3\pi \upsilon d_{h,i}} = \left(\frac{2\pi}{q^2}\right)\left(\frac{1}{\tau_i}\right)$$

where k_B, T, υ, and d_h are the Boltzmann constant, the absolute temperature, the (effective) viscosity of the solvent, and the hydrodynamic size, respectively, while $q = 2k_0 nsin(\theta/2)$ is the magnitude of the scattering vector, with $k_0 = \frac{2\pi}{\lambda_0}$ and $\theta = \pi\, rad$.

Thus, the contribution of each population to the total intensity of the dynamics, β, is

$$\beta = \sum_{i=1}^{3} \beta_i = \alpha \sum_{i=1}^{3} N_i \sigma_i$$

where σ_i and N_i the scattering cross-section and the number density of i-th dynamic elements.

3. Results

Hysteresis behavior of an isolated tubulin-MT system under assembly/disassembly through temperature modulation. We performed low-coherence dynamic light scattering (LC-DLS) measurements in a closed, *in vitro* tubulin-microtubule system (see Materials and Methods for details about the measurement system). The main advantage of using this technique is that one can continuously monitor both microscopic properties (size distribution) and an effective macroscopic property (turbidity) of the entire sample [17,21]. The initial tubulin sample has a total volume of 200 μL, which contains tubulin dimers, GTP and BRB80 buffer (see Materials and Methods for details about the sample preparation). A multimode optical fiber is immersed in the tubulin suspension (see Fig. 2a). The light reflected from the fiber-glass interface interferes with light scattered from the medium leading to measurable intensity fluctuations [22]. The finite coherence length (~30 μm) of the light source limits the scattering contributions to a layer of approximately 30 μm. This effective 'optical isolation' allows continuously monitoring the system during the polymerization/depolymerization process in spite of significant changes in its optical density. The initial temperature of the system was set at 2 °C to prevent possible polymerization. With temperature control ranging from 2 to 37 °C, depending on the temperature of the system, MTs will undergo either polymerization or depolymerization. Therefore, the state of such a system with free and polymerized tubulin will evolve accordingly. In our approach, two independent measurable quantities, the total energy in the intensity fluctuation, and the hydrodynamic sizes of each tubulin subpopulations, can be simultaneously retrieved as quantitative descriptors of the state of the system (see Materials and Methods). The total energy in the intensity fluctuations, which is denoted by β, is proportional to the total mass of polymerized tubulin units. This parameter is somewhat related to the so-called turbidity, a macroscopic measure of light attenuation that is widely used to quantify the optical density of liquid systems at steady state.

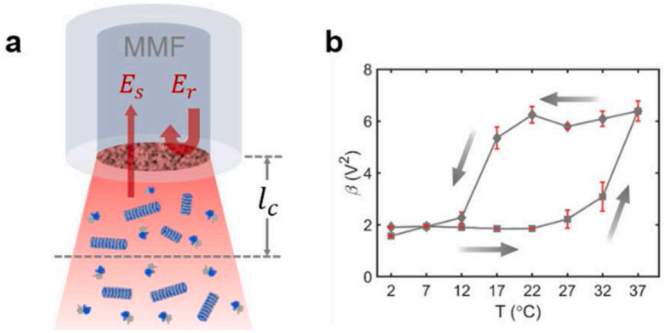

Fig. 2. Coherence-gated dynamic light scattering for tracking the MT polymerization/depolymerization process. a Schematic depiction of the fiber-based light scattering setup. The field E_s scattered from the sample within a volume gated by the coherence length of the source (l_c) interferes with the referenced E_r reflected from the fiber's end facet. This interference leads to measurable fluctuations of intensity. The information about the scattering system is retrieved from the power spectral density (PSD) of these intensity fluctuations. The PSD integral (total fluctuating energy β) defines the total amount of polymer mass contributing to the dynamic signal. **b** The measured total energy of intensity fluctuations β corresponding to a closed tubulin-MT system that evolves along a complete temperature cycle (arrow indicates the time evolution in the measurement). The error bars are standard deviation over 5 PSDs measured at each temperature.

To demonstrate the capability of our technique for resolving the state of the polymerizing system, we first carried out a measurement on the tubulin-MT system within one cycle, but with small temperature gradient. In the first half cycle, starting at 2 °C, we gradually increased the temperature with a step size of 5 °C, until it reached 37 °C. In the second half cycle, we followed a similar procedure, but with the decrease of temperature of the same step size until it dropped to 2 °C. At each temperature, we allowed the system to equilibrate for 5 min before proceeding with the dynamics measurements for a duration of 10 min (5 PSDs, 2 min for each PSD). We found that this time interval is sufficient for the temperature to stabilize, which is also discussed in Section 1 of the Supplementary Materials. The results are summarized in Fig. 2b, which shows how the total polymerized mass evolves in time. In the first half cycle, the total polymerized mass is negligible from 2 °C to 22 °C because of the low temperature. Starting at 27 °C, the polymerized mass starts to accumulate and it reaches the maximum value at 37 °C, which is the optimal and typical temperature for polymerizing MTs [23].

In the second half cycle, β remains relatively constant between 37 °C and 22 °C, which indicates that most of the tubulin dimers have been polymerized and the system has actually reached steady-state. Note that above 22 °C, the overall polymerization rate of the MT system is larger than the net rate of depolymerization. Below 22 °C, depolymerization starts to be the dominant mechanism. Therefore, the total polymerized mass decreases rapidly and the system eventually reaches the initial state. As can be seen in Fig. 2b, the amount of polymerized tubulin follows a hysteresis loop in this temperature cycling experiment. We note that a similar dependence with temperature has been observed previously in a qualitative examination of tubulin aggregation [24].

We also emphasize that, at each temperature step, the system might not reach its thermodynamic equilibrium for a given target temperature. However, as clearly seen in Fig. 2b, our technique is capable of resolving the temporal evolution of system state. Also, a hysteretic behavior of the closed tubulin-MT system within a temperature gradient cycle is evident. The features of such thermal hysteresis contain ample information about the supramolecular assembly process [25]. Due to a complicated energy landscape, the system does not react immediately to the externally applied thermodynamic variable, which, in this case, is ambient temperature. The transition between equilibrium states depends on the difference between the energy stored and released during the assembly/disassembly process.

In the following we address the next level questions about the tubulin-MT system: How will the system evolve over many cycles of temperature changes between equilibrium states of 2 °C and 37 °C? Will this hysteresis behavior remain the same?

Hysteresis phenomenon of an isolated tubulin-MT system: cyclical experiment. To answer the above questions, we designed a cyclical polymerization/depolymerization experiment. Samples were prepared following the same protocol as described above (also see Materials and Methods). Each sample was kept at 2 °C initially and then LC-DLS measurements were performed over 9 successive polymerization/depolymerization cycles. Each cycle is divided into two half cycles: the temperature-raising half cycle (from 2 °C to 37 °C) and the temperature-lowering half cycle (from 37 °C to 2 °C), respectively. Each half cycle lasts 25 min, making up for a total of 50 min per cycle (which corresponds to acquiring 100 PSDs, 30s integration time for each PSD). Measurements are not taken during the first 5 min in each half cycle to allow for temperature stabilization (See Supplementary Materials Section 1). The experimental results are summarized in Fig. 3.

The time trace of the value of parameter β in the first cycle of the measurement is shown in Fig. 3a. It is evident that polymerization occurs in the first half cycle, which corresponds to the increase of β (red line and arrow). The MTs depolymerization occurs in the second half cycle, where the decrease of β is apparent (blue line and arrow). This hysteresis phenomenon is similar to the one in Fig. 2b. The slight difference in the shape of the this hysteresis loop and the previous one can

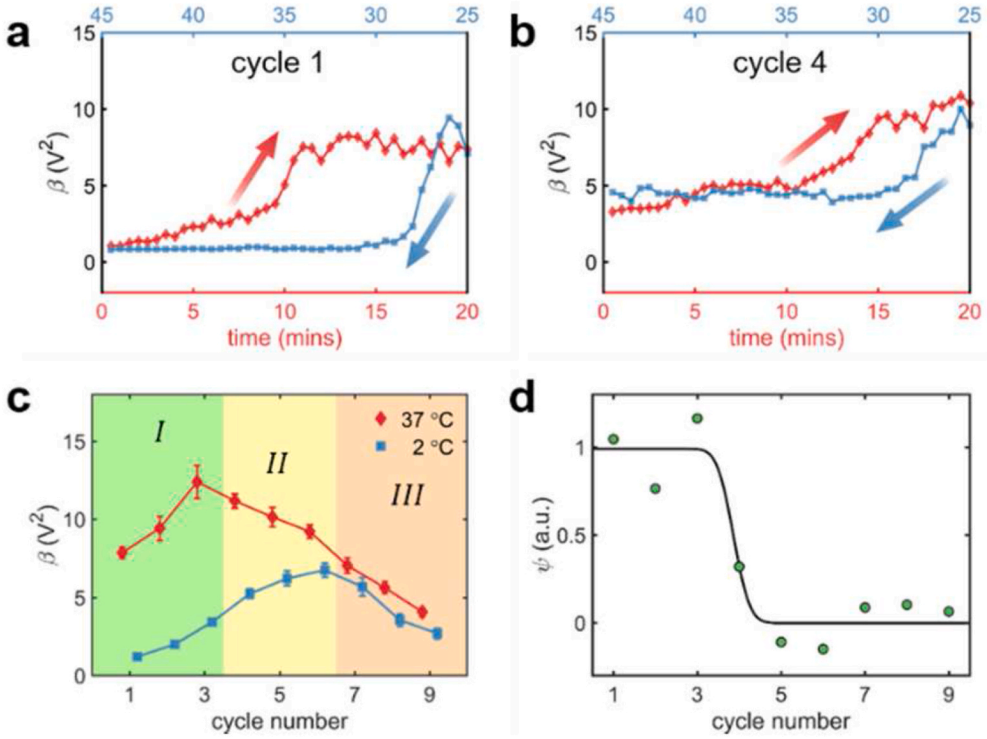

Fig. 3. Hysteresis analysis of an isolated tubulin-MT system. a-b Typical hysteresis curves for cycle 1 and 4 of the same system. The arrows indicate the time evolution of the temperature-raising/lowering process. **c** Evolution of the absolute values of β at steady-state for 2 °C and 37 °C, respectively, during nine temperature cycles. Three different regions can be identified for the hysteresis cycles, which are related to the different condition of the system (see text). **d** Evolution of the thermal hysteresis area Ψ (green dots) during the cyclical measurement illustrates the irreversibility of the MT assembly/disassembly process. The black curve is used for visual guiding only. (For interpretation of the references to color in this figure legend, the reader is referred to the Web version of this article.)

be associated to the fact that now only two temperatures (2 °C and 37 °C) are set in the current thermal cycle. Nevertheless, similar to previous observations, for cycle 1, β has the same value before and after a full cycle, meaning the system returns to its initial state. We would like to emphasize that the hysteresis behavior in Fig. 3a is not directly comparable with the example shown Fig. 2b because the experimental design is quite different. For Fig. 3a as well as the data shown later on, we are concerned with the system evolution at the two stabilized temperatures of 2 °C and 37 °C. The transition between these limits is more rapid than for the cycle illustrated in Fig. 2b where the temperature increases slowly, which makes the assembly/disassembly process to proceed at different rates.

Surprisingly, we observed a quite different hysteresis loop compared to the first cycle when the experiment proceeds, meaning this hysteresis effect evolves differently during the experiment. As an example, Fig. 3b illustrates the evolution of the same sample during the fourth cycle. First, the area between the two curves (denoted by Ψ) is much smaller compared to one in the first cycle. This means that the change of the total polymerized mass within one cycle has decreased. Also, β no longer returns to its value at the beginning of the fourth cycle, which indicates that at least some of the MTs are not completely depolymerized anymore at the end of this cycle.

To further quantify the evolution of the hysteresis process, the value of β measured at steady-state during the last 5 min in each half cycle are summarized in Fig. 3c for all the cycles in the experiment. Three different regions can be identified in the evolution of β. Cycle 1 to 3, region I, with β increasing both at low and high temperatures corresponds to a regime where MTs have been consistently polymerized (at 37 °C) and depolymerized (at 2 °C). Due to the relatively short time for half a cycle (25 min), MTs are not completely depolymerized at 2 °C. Therefore, we observed different values of β within region I. In region II that covers the cycles 4 to 6, MTs are still elongating at 37 °C, since the value of β at this temperature is much larger than β at 2 °C. However, the absolute value of β at 37 °C is decreasing, which means that although both polymerization and depolymerization are playing a role, the rate of polymerization at 37 °C is lower than the depolymerization one at 2 °C. Finally, from cycle 7 to 9, the values of β at both temperatures are rather close. The reason why β at 37 °C is slightly larger than at 2 °C is due to the fact that the same polymer system is more dynamic at high temperatures. In this region III, the polymerization is minimal, while some depolymerization events are still taking place as not all the MTs are depolymerized yet. In other words, at the macroscopic scale, there are no new MTs being polymerized. The system is dominated by depolymerization effects, which have been consistently decreasing the values of β in these three cycles. A similar conclusion can be inferred from Fig. 3d, where we plot the change of total mass $\Psi = \int_{20}^{t_{37}} \beta(t)dt - \int_{t_{25}}^{45} \beta(t)dt$ in each cycle. The evolution of this thermal hysteresis parameter Ψ during the cyclical measurement on an isolated tubulin-MT system clearly illustrates the irreversibility of the MT assembly/disassembly process.

Based on the results of these experiments, it can be concluded that the hysteresis phenomenon in the temperature cycling of a tubulin-MT system is not a stationary process. Instead, it highly depends on the number of polymerization/depolymerization events that the system experienced during the process. After several cycles, the polymerization/depolymerization cannot be observed anymore. Next, we will explain the reason for this observation based on further analysis of the dynamics of light scattering measurements. In particular, it is important to understand if the eventual inability to polymerize MTs is due to the loss of GTP that is required for tubulin assembly or due to other reasons such, for instance, the aging of the protein after being subjected to thermal cycles heating and cooling.

Size distribution evolution during the cyclical experiment. As discussed in the previous section, our LC-DLS technique allows us to simultaneously determine an effective optical density (turbidity) and the hydrodynamic sizes of the suspended scattering centers. Therefore, in this section, we performed a detailed analysis of the size distribution of the scattering elements within the tubulin-MT system and traced it over the entire duration of the multi-cycle experiment.

Fig. 4a illustrates the principle of retrieval of hydrodynamic sizes in our PSD measurement (the PSD at 37 °C in the first cycle is used as an example here, while others are shown in the Supplementary Materials

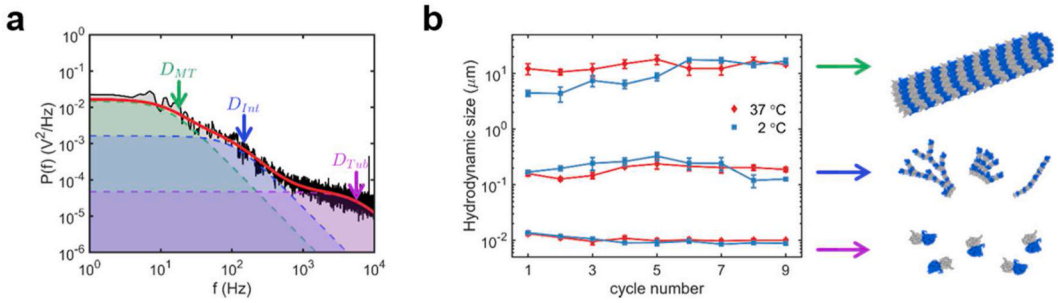

Fig. 4. Size distribution within the tubulin-MT system. a Measured PSD (black curve) decomposition into three independent Lorentzian spectra corresponding to three different size groups corresponding to MTs, intermediate aggregates (MT sheets, tubulin oligomers, tubulin clusters, etch), and tubulin dimers. The effective hydrodynamic size of each component is evaluated from the corresponding corner frequency. Red curve illustrates the summation over three size groups. **b** Evolution of the hydrodynamic size of three populations during the multi-cycle experiment. The increase of the hydrodynamic length of MT at 2° (blue curve on top) over cycles is evident. The error bars represents the standard deviations over 10 PSDs at equilibrium stage of each cycle. (For interpretation of the references to color in this figure legend, the reader is referred to the Web version of this article.)

Section 2). First, the experimentally acquired PSD (black line) is decomposed into a collection of multiple Lorentzian functions [21]. Each Lorentzian function corresponds to a diffusion coefficient of a group of mono-dispersed scattering elements. For the current system, three such Lorentzian functions can properly describe the PSD (see Materials and Methods). The first one (green dashed line), which has the lowest corner frequency, relates to the combined translational and longitudinal diffusion coefficient of the MTs. The one with largest corner frequency (pink dashed line), is mainly indicative of the diffusion coefficient of tubulin dimers. The intermediate component, which has a corner frequency of around 200 Hz (blue dashed line), corresponds to scattering elements having a hydrodynamic size of approximately one hundred nanometers. Although it is not straightforward to interpret this length scale from a scattering measurement, literature reports indicate the presence of intermediate tubulin aggregates of similar sizes, such as tubulin dimer clusters, tubulin oligomers, short MTs, or even tubulin dimer sheets [26–30]. We note that, to accurately describe an experimentally measured PSD, one has to account for the specific intermediate diffusion coefficients. In our case, the summation of these three Lorentzian functions (red line) describes the PSD reasonably well for the entire duration of the experiment.

Next, the effective hydrodynamic size of each population is extracted from the corner frequency of the corresponding PSD component. For MTs, its hydrodynamic length can be calculated from a diffusion model [31] as its diameter of this cylindrical structure is already known (25 nm). The results are summarized in Fig. 4b, where the cartoon on the right-hand side indicates the element contributing to that particular size. The value and the error bars are the mean and standard deviation of the hydrodynamic size from the last 5 min in each half cycle, respectively.

The two curves on top denote the average hydrodynamic length of the MTs at two different temperatures in each cycle. It is clear that at the steady state of each cycle, the length of MTs at 37 °C is already larger than 10 μm and no significant difference occur during all cycles. This means that MTs are polymerized effectively at 37 °C. We note that, as opposed to other reported data, such as, for instance, Refs. [32,33], this effective size recovered in our experiments constitutes the average hydrodynamic diameter, which is different from the physical size and is also solvent dependent. At 2 °C, MTs are initially much shorter, meaning they depolymerize at low temperatures. However, with increasing the number of cycles, the length of MTs keeps increasing and eventually becomes similar to the 37 °C case. In other words, the length of MTs at 37 °C is larger than at 2 °C (for the first 5 cycles), which indicates that the polymerization rate is higher than the depolymerization rate. For the last 4 cycles, the length of MTs does not change, meaning both the polymerization and depolymerization processes cease. These observations correlate with the previous analysis of β in Fig. 3c–d.

A few more interesting observations can be made regarding the two curves corresponding to intermediate sizes. It can be seen that the size of this contribution increases during the first five cycles and then decreases for the last few cycles. This indicates that the immediate aggregates are not depolymerized efficiently until closed to the end of the experiment. Also, overall, the hydrodynamic size at 2 °C is larger than at 37 °C. This is attributed to the additional contribution from the tubulin sheets or stable oligomers at low temperature.

The last two curves correspond to the tubulin dimers, which maintain a size of approximately 9–11 nm for the entire duration. This value is slightly larger than the actual physical size of the tubulin dimer (5nm × 4 mm × 8 nm) [34], possibly because it also includes a contribution from some oligomers and the rotational diffusion coefficient of the MTs [35].

Polymerization/Depolymerization rate evolution during the cyclical experiment. Since we can distinguish the size of these three populations of tubulin, it is also critical to determine the contribution of each population to the overall value of β in Fig. 3c. The approach used to this end is detailed in Materials and Methods and the results are summarized in Fig. 5. In Fig. 5a–f we illustrate the evolution of β contributions from MTs and intermediate aggregates during three representative cycles. In each figure, the dots represent the experimental data while the continuous lines indicate the result of a linear fitting of β with confidence bounds represented by the color backgrounds. Since the process is nonlinear for the first cycle (a similar trend is observed in traditional turbidity assays), the polymerization processes (red) are fitted only for data acquired during 10 min in the middle (6–15 min), while the depolymerization process (blue) are fitted only with the data for the initial 5 min (23–27 min). For Fig. 5a–c, it is evident that the polymerization and depolymerization rate of MTs (slope of the fitting line) are both decreasing. A similar observation applies for the intermediate aggregates, in Fig. 5d–f. Similar figures for tubulin dimers are not shown because their contribution to the overall β is both smaller and invariant, either within one cycle or between different cycles.

The polymerization and depolymerization rates for all three contributing tubulin populations are calculated and shown in Fig. 5g and h, respectively. When calculating these rates, we considered that, due to high polymerization efficiency in the first three cycles, all the tubulin dimers have been polymerized at the stage when the measurement gives highest β (in the third cycle) [36]. The scattering cross-sections of each population were evaluated from the corresponding hydrodynamic sizes. We also considered that the polymerization and depolymerization effect is the net result of averaging over all MTs inside the system.

As can be seen in Fig. 5g, for the first three cycles, the MTs polymerization rate is approximately 0.5 μm/min while the depolymerization rate is − 1.8 μm/min. These values change during the subsequent cycles and tend to zero at the end of the experiment. If we considered the

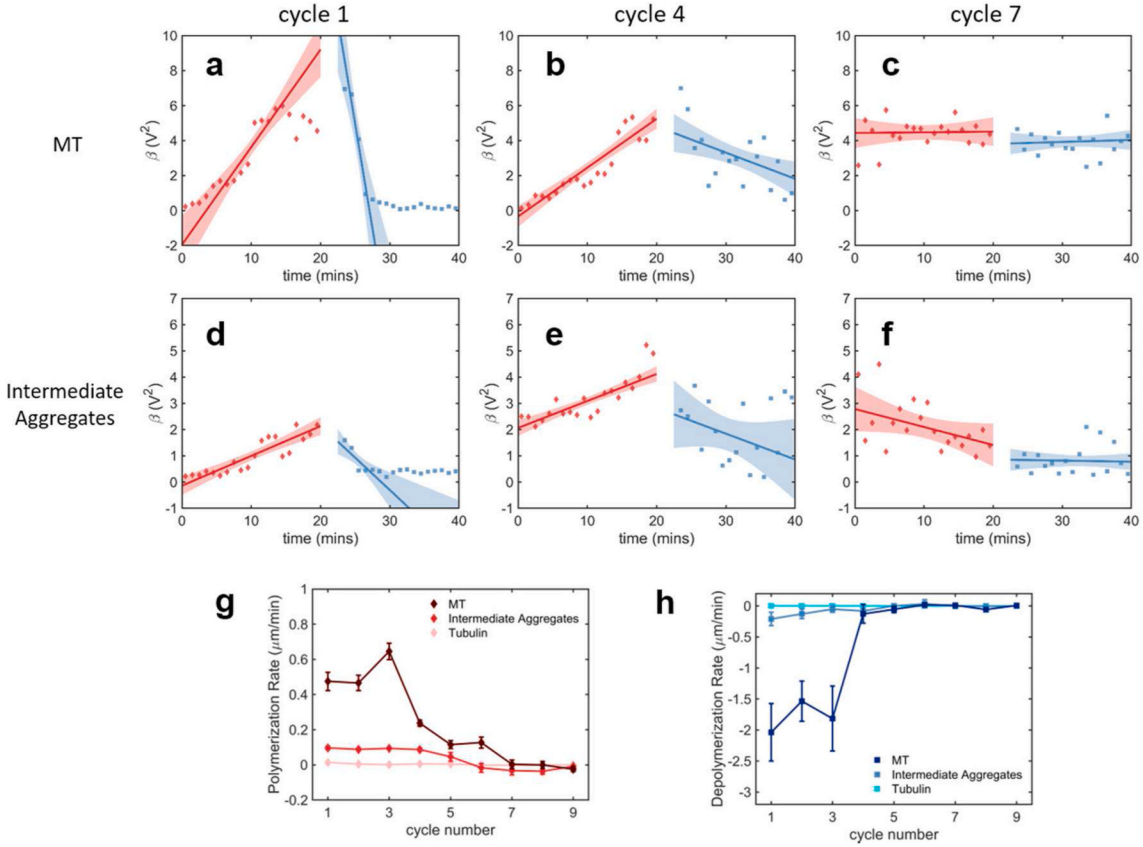

Fig. 5. Hysteresis analysis of the cyclical experiment for different populations inside the system. a-c Hysteresis behavior of aggregated MT during temperature increasing/decreasing in three different cycles as indicated. **d-f** Hysteresis behavior of intermediate aggregates during temperature increasing/decreasing for three different cycles, respectively. The rates of polymerization and depolymerization are denoted by the slope of the fitting in each cycle, respectively. The colored regime indicates the confidential bounds of the fitting. **g-h** Evolution of polymerization (g) and depolymerization (h) rates for three tubulin populations. The error bars represents the fitting error of the linear regression slope.

intermediate aggregates to be ring-type, we find that their initial rates are smaller and in the order of 0.1 μm/min and −0.2 μm/min for the polymerization and depolymerization, respectively. These values also gradually decrease to zero towards the end of the experiment. To the best of our knowledge, this is the first time that the polymerization and depolymerization rates for the intermediate tubulin aggregates are reported. Notably, at cycle 4–5, both the polymerization and the depolymerization rates are similar for these two populations. This indicates that the intermediate aggregate population contributes significantly to the value of β starting with cycle 4, which is exactly what is seen in Fig. 5b and e. Also, the rate of the intermediate aggregates are negative from cycle 6 to 8, which is due to the disassembly of ring-type structures [37].

The results summarized in Fig. 5 are consistent with the phase transition shown in Fig. 3c–d. In the first three cycles, the hysteresis curve does not change significantly. Starting from cycle 4, the intermediate aggregates start to play an important role, and they do not depolymerize as easily as the MTs. As these intermediate structures are accumulated in the system, a smaller number of MTs would be formed and eventually the rate of MT assembly goes down to zero (Fig. 5g). Therefore, we can conclude that the intermediate aggregates of tubulin are the origins of the "aging" of tubulin dimers. After several polymerization-depolymerization cycles, the tubulin dimers can only form "faulty" (i.e. MT assembly incompetent) structures instead of properly structured MTs.

4. Discussion

We reported the results of assembly/disassembly of MTs from an unpolymerized pool of tubulin subjected to cycles of temperature increase to 37 °C followed by decreasing the temperature down to 2 °C. During this cyclical process, a number of distinctive effects have been identified for the first time. First, a pronounced hysteresis loop in terms of polymerized mass of tubulin as a function of temperature has been clearly seen. This is consistent with earlier observations of a phase diagram for tubulin and MTs [38], which was elucidated in terms of phase transitions of the first order between free tubulin and MTs in a Landau-Ginzburg based model [19]. It is a well-known property of systems undergoing first order phase transitions that they are associated with thermal hysteresis loops [39]. In contrast, second order phase transitions only show field-induced hysteresis. The size of the hysteresis loop in terms of the temperature range corresponds to the range of co-existence between the two metastable phases. At the lower temperature end of the loop the free tubulin phase is absolutely stable and MTs become unstable while at the upper temperature end, the assembled tubulin phase (MTs) is absolutely stable and free tubulin state becomes unstable. However, this idealized picture of physical systems undergoing similar phase transitions is only partially applicable in the case of tubulin, a biological system. We have discovered the presence of an intermediate state which is comprised of neither free tubulin nor polymerized MTs, but rather clusters, oligomers or sheets of tubulin which appear to persist without either breaking down into unpolymerized tubulin or reassembling into MTs.

Another important effect that emerged in this study is the property of tubulin aging. Following several cycles of polymerization and depolymerization of tubulin, a large fraction of the protein is no longer capable of polymerizing into MTs. This is not a result of the depletion of the pool of GTP, since the concentration of GTP used was over 20 times greater

than that of tubulin, hence several cycles of polymerization would not consume more than half of the available GTP pool. Instead, we hypothesize that tubulin undergoes structural deterioration making it assembly incompetent, even if it binds GTP. This is also consistent with previously reported work, including reports of age-dependent MT catastrophe effects [13,14,40] and MT end-taper as a function of age [16]. Similar conclusions were reached in a microfluidic study of MTs [41].

Our results not only implicate aging of the tubulin material in the MT tip structure but also in the assembly process itself and point to an inability of tubulin to form MTs after fewer than 10 cycles of assembly and disassembly. It is not entirely clear if these effects are due to the mechanical "wear and tear" involved in the binding and unbinding reactions or due to thermally-induced damage. A close examination of the structural changes in tubulin following temperature cycling using, for example X-ray crystallography [42], would provide direct information about the root cause of these effects. Potential implications on human physiology, including the origin of disease of aging, such as Alzheimer's and cancer, are enormous. Especially in the case of Alzheimer's neuronal MT damage is in clear evidence, although primarily due to hyperphosphorylation of microtubule associated protein (MAP) tau [43]. Nonetheless, a contributing factor to the onset of this disease could be the decreased ability of old tubulin to form MTs.

A less direct but potentially equally important connection may exist between tubulin aging and cancer. Aneuploidy, an unbalanced complement of chromosomes, is one of the common manifestations of the cancer phenotype in cells. There exists a direct link between aneuploidy and abnormal MT dynamics as recently reported by Böhly et al. [44]. Since MTs form mitotic spindles in all eukaryotic cells and since cell division occurs commonly more frequently in cancer cells than normal cells, recycling of "old" tubulin by cancer cells may be a contributing factor to the onset of the disease.

Finally, it must be stressed that additional studies are required to address the issue of the morphology of the various supramolecular tubulin structures generated in the process of thermal hysteresis. The techniques used in the present study are not able to precisely identify the various forms of tubulin organization.

Author contributions

R.W. and J.R.G.-S. performed the experiments, processed, and analyzed data. A.D. and J.A.T. conceived the research. A.D. directed the project. All authors contributed to analyzing the results writing the paper.

Declaration of competing interest

The authors declare no conflict of interest.

Acknowledgements

The authors thank Kyu Young Han for suggestions with the experiment. The research was partially supported by the Defense Advanced Research Projects Agency (DARPA). J.A.T. acknowledges funding support from NSERC (Canada).

Appendix A. Supplementary data

Supplementary data to this article can be found online at https://doi.org/10.1016/j.bbrep.2021.101199.

References

[1] F. Gittes, B. Mickey, J. Nettleton, J. Howard, Flexural rigidity of microtubules and actin filaments measured from thermal fluctuations in shape, JCB (J. Cell Biol.) 120 (4) (1993) 923–934.
[2] S.L. Kline-Smith, C.E. Walczak, Mitotic spindle assembly and chromosome segregation: refocusing on microtubule dynamics, Mol. Cell 15 (3) (2004) 317–327.
[3] Lukas C. Kapitein, Casper C. Hoogenraad, Building the neuronal microtubule Cytoskeleton, Neuron 87 (3) (2015) 492–506.
[4] B.Y. Monroy, T.C. Tan, J.M. Oclaman, J.S. Han, S. Simó, S. Niwa, D. W. Nowakowski, R.J. McKenney, K.M. Ori-McKenney, A combinatorial MAP code dictates polarized microtubule transport, Dev. Cell 53 (1) (2020) 60–72, e64.
[5] M. Burute, L.C. Kapitein, Cellular logistics: unraveling the interplay between microtubule organization and intracellular transport, Annu. Rev. Cell Dev. Biol. 35 (1) (2019) 29–54.
[6] K.S. Burbank, T.J. Mitchison, Microtubule dynamic instability, Curr. Biol. 16 (14) (2006) R516–R517.
[7] T. Mitchison, M. Kirschner, Microtubule assembly nucleated by isolated centrosomes, Nature 312 (5991) (1984) 232–237.
[8] A. Desai, T.J. Mitchison, Microtubule polymerization dynamics, Annu. Rev. Cell Dev. Biol. 13 (1) (1997) 83–117.
[9] T. Mitchison, M. Kirschner, Dynamic instability of microtubule growth, Nature 312 (5991) (1984) 237–242.
[10] V. VanBuren, D.J. Odde, L. Cassimeris, Estimates of lateral and longitudinal bond energies within the microtubule lattice, Proc. Natl. Acad. Sci. Unit. States Am. 99 (9) (2002) 6035–6040.
[11] E.T. O'Brien, W.A. Voter, H.P. Erickson, GTP hydrolysis during microtubule assembly, Biochemistry 26 (13) (1987) 4148–4156.
[12] D.N. Drechsel, M.W. Kirschner, The minimum GTP cap required to stabilize microtubules, Curr. Biol. 4 (12) (1994) 1053–1061.
[13] Melissa K. Gardner, Blake D. Charlebois, Imre M. Jánosi, J. Howard, Alan J. Hunt, David J. Odde, Rapid microtubule self-assembly kinetics, Cell 146 (4) (2011) 582–592.
[14] M.K. Gardner, M. Zanic, J. Howard, Microtubule catastrophe and rescue, Curr. Opin. Cell Biol. 25 (1) (2013) 14–22.
[15] A. Akhmanova, M. Dogterom, Kinesins lead aging microtubules to catastrophe, Cell 147 (5) (2011) 966–968.
[16] Courtney E. Coombes, A. Yamamoto, Madeline R. Kenzie, David J. Odde, Melissa K. Gardner, Evolving tip structures can explain age-dependent microtubule catastrophe, Curr. Biol. 23 (14) (2013) 1342–1348.
[17] J. Guzman-Sepulveda, A. Dogariu, Probing complex dynamics with spatiotemporal coherence-gated DLS, Appl. Opt. 58 (13) (2019) D76–D90.
[18] L.U. Cassimeris, P. Wadsworth, E.D. Salmon, Dynamics of microtubule depolymerization in monocytes, JCB (J. Cell Biol.) 102 (6) (1986) 2023–2032.
[19] D. Sept, J.A. Tuszyński, A Landau-Ginzburg model of the Co-existence of free tubulin and assembled microtubules in nucleation and oscillations phenomena, J. Biol. Phys. 26 (1) (2000) 5–15.
[20] J. Guzman-Sepulveda, R. Argueta-Morales, W. DeCampli, A. Dogariu, Real-time intraoperative monitoring of blood coagulability via coherence-gated light scattering, Nat. Biomed. Eng. 1 (2) (2017) 1–6.
[21] I. Sohn, R. Rajagopalan, A. Dogariu, Spatially resolved microrheology through a liquid/liquid interface, J. Colloid Interface Sci. 269 (2) (2004) 503–513.
[22] G. Popescu, A. Dogariu, Dynamic light scattering in localized coherence volumes, Opt. Lett. 26 (8) (2001) 551–553.
[23] J. Olmsted, G. Borisy, Characterization of microtubule assembly in porcine brain extracts by viscometry, Biochemistry 12 (21) (1973) 4282–4289.
[24] U. Spann, W. Renner, E.M. Mandelkow, J. Bordas, E. Mandelkow, Tubulin oligomers and microtubule assembly studied by time-resolved X-ray scattering: separation of prenucleation and nucleation events, Biochemistry 26 (4) (1987) 1123–1132.
[25] N. Avakyan, H.F. Sleiman, A.K. Mittermaier, Mapping the energy landscapes of supramolecular assembly by thermal hysteresis, Nat. Commun. 9 (1) (2018) 1–10.
[26] N. Caudron, I. Arnal, E. Buhler, D. Job, O. Valiron, Microtubule nucleation from stable tubulin oligomers, J. Biol. Chem. 277 (52) (2002) 50973–50979.
[27] J. Mozziconacci, L. Sandblad, M. Wachsmuth, D. Brunner, E. Karsenti, Tubulin dimers oligomerize before their incorporation into microtubules, PLoS One 3 (11) (2008), e3821.
[28] S.R. Norris, S. Jung, P. Singh, C.E. Strothman, A.L. Erwin, M.D. Ohi, M. Zanic, R. Ohi, Microtubule minus-end aster organization is driven by processive HSET-tubulin clusters, Nat. Commun. 9 (1) (2018) 2659.
[29] S.G. Wolf, G. Mosser, K.H. Downing, Tubulin conformation in Zinc-induced sheets and macrotubes, J. Struct. Biol. 111 (3) (1993) 190–199.
[30] A.P. Kalra, S.D. Patel, B.B. Eakins, S. Riddell, P. Kumar, P. Winter, J. Preto, K. W. Carlson, J.D. Lewis, V. Rezania, Revealing and attenuating the electrostatic properties of tubulin and its polymers, Small 17 (1) (2021) 2003560.
[31] B. Bhaduri, A. Neild, T.W. Ng, Directional Brownian diffusion dynamics with variable magnitudes, Appl. Phys. Lett. 92 (8) (2008), 084105.
[32] Y. Jeune-Smith, H. Hess, Engineering the length distribution of microtubules polymerized in vitro, Soft Matter 6 (8) (2010) 1778–1784.
[33] M.-F. Carlier, Kinetic evidence for a conformation change of tubulin preceding microtubule assembly, J. Biol. Chem. 258 (4) (1983) 2415–2420.
[34] J.A. Tuszynski, E.J. Carpenter, J.T. Huzil, W. Malinski, T. Luchko, R.F. Luduena, The evolution of the structure of tubulin and its potential consequences for the role and function of microtubules in cells and embryos, Int. J. Dev. Biol. 50 (2–3) (2003) 341–358.
[35] A.P. Kalra, P. Kar, J. Preto, V. Rezania, A. Dogariu, J.D. Lewis, J.A. Tuszynski, K. Shankar, Behavior of α, β tubulin in DMSO-containing electrolytes, Nanoscale Adv. 1 (9) (2019) 3364–3371.

[36] C.L. Bokros, J.D. Hugdahl, V.R. Hanesworth, J.V. Murthy, L.C. Morejohn, Characterization of the reversible taxol-induced polymerization of plant tubulin into microtubules, Biochemistry 32 (13) (1993) 3437–3447.
[37] J. Bordas, E.-M. Mandelkow, E. Mandelkow, Stages of tubulin assembly and disassembly studied by time-resolved synchrotron X-ray scattering, J. Mol. Biol. 164 (1) (1983) 89–135.
[38] D.K. Fygenson, E. Braun, A. Libchaber, Phase diagram of microtubules, Phys. Rev. E 50 (2) (1994) 1579–1588.
[39] K. Binder, Theory of first-order phase transitions, Rep. Prog. Phys. 50 (7) (1987) 783–859.
[40] D.J. Odde, L. Cassimeris, H.M. Buettner, Kinetics of microtubule catastrophe assessed by probabilistic analysis, Biophys. J. 69 (3) (1995) 796–802.
[41] C. Duellberg, N.I. Cade, T. Surrey, Microtubule aging probed by microfluidics-assisted tubulin washout, MBoC 27 (22) (2016) 3563–3573.
[42] A. Dorleans, M. Knossow, B. Gigant, Studying Drug-Tubulin Interactions by X-Ray Crystallography, Springer, 2007, pp. 235–243. Microtubule Protocols.
[43] T.J.A. Craddock, J.A. Tuszynski, D. Chopra, N. Casey, L.E. Goldstein, S. R. Hameroff, R.E. Tanzi, The Zinc dyshomeostasis hypothesis of Alzheimer's disease, PLoS One 7 (3) (2012), e33552.
[44] N. Böhly, M. Kistner, H. Bastians, Mild replication stress causes aneuploidy by deregulating microtubule dynamics in mitosis, Cell Cycle 18 (20) (2019) 2770–2783.